

Disorder-induced spin-cluster ferrimagnetism in a doped kagome spin liquid candidate

Arnab Seth¹, Joseph C. Prestigiacomo², Aini Xu³, Zhenyuan Zeng^{3,4}, Trevor D. Ford⁵, B.S. Shivaram⁵, Shiliang Li^{3,4,6}, Patrick A. Lee⁷, and Itamar Kimchi¹

¹*School of Physics, Georgia Institute of Technology, Atlanta, Georgia 30332, USA.*

²*Materials Science and Technology Division, Naval Research Laboratory, Washington, DC 20375, USA.*

³*Beijing National Laboratory for Condensed Matter Physics,*

Institute of Physics, Chinese Academy of Sciences, Beijing 100190, China.

⁴*School of Physical Sciences, University of Chinese Academy of Sciences, Beijing 100190, China.*

⁵*Department of Physics, University of Virginia, Charlottesville, Virginia 22904, USA.*

⁶*Songshan Lake Materials Laboratory, Dongguan, Guangdong 523808, China and*

⁷*Department of Physics, Massachusetts Institute of Technology, Cambridge, Massachusetts 02139, USA.*

(Dated: November 18, 2024)

The search for new quantum spin liquid materials relies on systems with strong frustration such as spins on the kagome lattice. This allows lattice imperfections to have substantial effects which are not well understood. In recent work the 2D kagome system $\text{YCu}_3(\text{OH})_6[(\text{Cl}_x\text{Br}_{1-x})_{3-y}(\text{OH})_y]$ has emerged as a leading candidate hosting a Dirac spin liquid which appears to survive at least for $x < 0.4$, associated with alternating-bond hexagon (ABH) disorder. Here in samples with $x = 0.58$ we report an unusual coexistence of anti-ferromagnetic (AFM) and ferromagnetic (FM) order, and propose a semi-microscopic model to account for this order. Combined with a phenomenological model the results suggest growth of large FM clusters at intermediate temperatures which order eventually at lower temperatures. Generating these FM clusters relies on two ingredients: ABH disorder, and local-AFM FM-canting generated by small Kitaev interactions which can arise on the kagome lattice. The combination of experimental observation and theory suggests that Kitaev interactions and ABH disorder are necessary for describing the magnetic fluctuations in this family of materials, with potential implications for the proposed proximate spin liquid phase.

PACS numbers: 75.30.Mb, 71.27.+a, 75.25.Dk

I. INTRODUCTION

Recently a new class of quantum kagome antiferromagnet (AFM) materials has been explored that minimize accidental substitutional disorder: $\text{YCu}_3(\text{OH})_6\text{Cl}_3$ [1–3]. Site mixing of magnetic and non-magnetic atoms is suppressed by their large difference in ionic radii. Rather than the sought after quantum spin liquid state this compound appears to harbor a magnetic phase transition [4, 5]. Since this system is well described by the 2D nearest-neighbor kagome AFM model (with Heisenberg exchange of order 100 K) where no magnetic transition is expected, the magnetic order is likely created by additional out-of-plane Dzyaloshinskii-Moriya (DM) interaction [6–9]. A partial substitution of Cl by O, giving the compound $\text{YCu}_3(\text{OH})_6\text{O}_x\text{Cl}_{(3-x)}$ with $x=1/3$, results in the absence of static magnetic order [10]. However, it is not clear what is the role of the O substitution, and in particular what is the correct microscopic description of the system and the substitution-induced disorder.

More recently a related family of compounds has been discovered, and some members of the family are shown not to order down to 50 mK. This family involves two doping parameters. First, the Cl in the kagome compound can be replaced by a combination of Br and OH [11–15], resulting in $\text{YCu}_3(\text{OH})_6\text{Br}_2[\text{Br}_{1-y}(\text{OH})_y]$, which we will refer to as YCOB. Second, YCOB is expanded into a family of compounds via partial replacement of Br by Cl, leading to $\text{YCu}_3(\text{OH})_6[(\text{Cl}_x\text{Br}_{1-x})_{3-y}(\text{OH})_y]$,

which we denote as YCOB-Cl [16, 17]. Extensive studies of the heat capacity C and linear magnetic susceptibility χ in high quality single crystals of this system for low x show behavior such as C/T with linear- T behavior at low T , that increases in magnetic fields H with a linear- H term beyond a threshold field, [14, 18, 19] consistent with a Dirac spin liquid [20, 21].

These compounds are reported to host a special type of disorder, where OH substitutes the Br sites randomly above and below the kagome hexagons formed by Cu atoms [16, 18]. This leads to alternating pattern of spin exchange interaction strength around that hexagon, resulting in *alternating-bond hexagon* (ABH) defects. Similar kind of disorder is found in the Ykapellasite $\text{Y}_3\text{Cu}_9(\text{OH})_{19}\text{Cl}_8$ [10, 22, 23]. It is not clear how ABH disorder impacts the magnetic properties of YCOB-Cl.

Here we present comprehensive measurements on samples with Cl concentrations large enough such that an AFM ordered state is observed [16]. A phenomenological model involving clusters of spins is presented to account for the data. Our analysis provides conclusive evidence that ferromagnetic (FM) clusters appear below T_N and thus throw additional light on the nature of the ordering transition. We then also present a comprehensive theory for generating these FM clusters, relying on two ingredients: alternating-bond hexagon (ABH) disorder, and local-order FM canting generated by small Kitaev-type interactions. The combination of experimental observa-

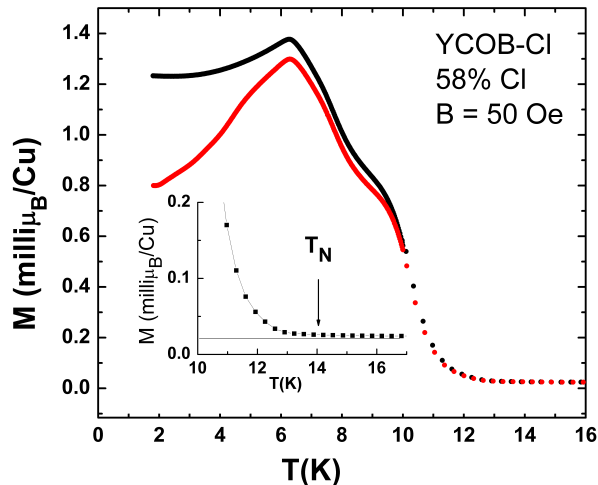


FIG. 1. The temperature dependence of the magnetization M for the 58% chlorine doped sample under FC and ZFC conditions (main panel) under a field of 50 Oe parallel to the hexagonal plane. The separation between the two curves is most prominent below 10 K and suggests formation of ferromagnetic clusters at this temperature. The inset is the same data on an expanded scale to demonstrate that a deviation from paramagnetic behavior sets in at 14 K.

tion and theory suggests that kagome Kitaev-type interactions arise and are necessary ingredient, together with ABH disorder, for describing the magnetic fluctuations in this family of materials.

II. EXPERIMENTAL FINDINGS AND PHENOMENOLOGY FROM SPIN CLUSTERS

Here we use single crystals of YCOB-Cl, $\text{YCu}_3(\text{OH})_6[(\text{Cl}_x\text{Br}_{1-x})_3-y(\text{OH})_y]$, which are grown using a similar hydrothermal method as described in reference [14]. This method allows to continuously tune the ratio between Cl and Br. The Cl-doped samples are obtained as hexagonal plates with the in-plane diameter up to 1.3 mm and thickness of 1 mm. To remove the possible surface impurities, all the crystals are cleaned ultrasonically in water. Magnetization measurements are performed on a Quantum Design magnetic property measurement system employing a sample holder traversing both halves of the static SQUID detection coils to eliminate any background contribution.

In Fig. 1 we show the magnetization as a function of temperature under both field cooled and zero field cooled conditions measured on a sample with 58% chlorine. The magnetization starts to rise at the transition to the AFM state, ≈ 14 K, and a discernible change in slope occurs around 7 K. Furthermore, the field cooled and zero field cooled curves separate below ≈ 10 K, indicating hysteretic behavior which is usually associated with ferromagnetism. This hysteresis is occurring for fields in the plane. The separation is initially very small but opens

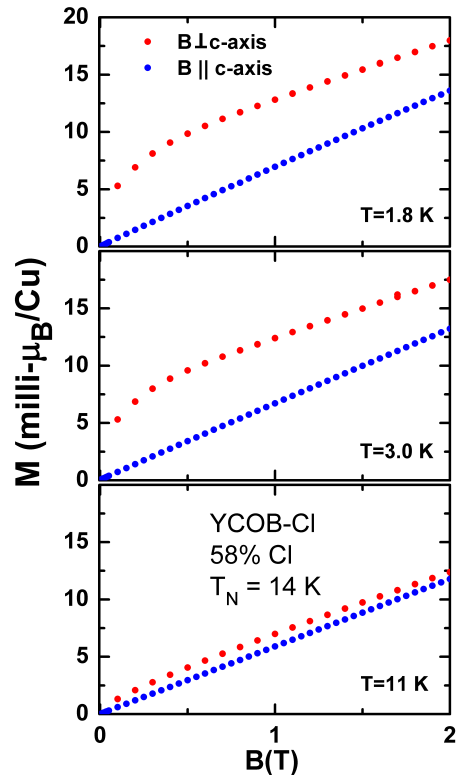


FIG. 2. Magnetization isotherms obtained at three different temperatures below T_N . For B parallel to the plane a clear ferromagnetic response suggesting saturation at a fairly low field is visible. Two separate linear regions, a low field region with a larger slope and high field linear response with a smaller slope are clearly seen. As $T \rightarrow T_N$ the low field response shrinks and is absent above the ordering temperature. In the perpendicular case, $B \parallel c$ -axis, no such ferromagnetic behavior is seen. The ordered moment per site is of the order $0.01 \mu_B$.

up below ≈ 7 K. We interpret this as the onset of large well ordered ferromagnetic regions which initially occupy a small volume fraction of the sample at 10 K. These regions grow and overlap to form a bulk FM below 7 K. We will refer to 7 K loosely as the FM long range order temperature. It is puzzling that this behavior is very different from what is expected for an AFM, which shows a cusp in the magnetic susceptibility at the Neel temperature.

In Fig. 2, we present the isotherms of M obtained at three different temperatures as shown. The isotherms for B parallel to plane exhibit a dual slope response - with an initial rapid rise which fades away as the temperature is raised towards T_N . These isotherms suggests a model where clusters consisting of ferromagnetically coupled spins contribute to the rapid rise but soon attain a saturated state. Fig. 3 shows the implied ordered moment, which is in the plane. Beyond saturation at higher fields there is a separate contribution to the magnetization arising from the antiferromagnetic coupling of the spins. Phenomenologically, these features can be cap-

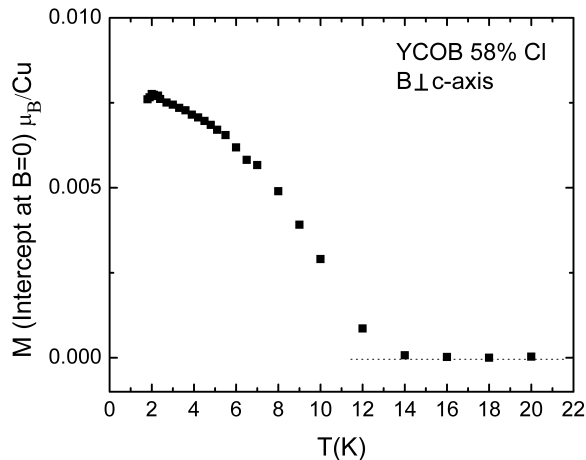


FIG. 3. Shows the implied ordered moment as obtained from an extrapolation of the high field linear behavior to obtain a $B = 0$ intercept. The data implies a net ordered moment in the plane.

tured using the following equation for the magnetization M :

$$M = n_c g S_{\text{eff}} \mu_B L \left(\frac{g S_{\text{eff}} \mu_B B}{k_B T} \right) + \chi_{\text{AF}} B \quad (1)$$

In this equation the magnetic response is split into two components: the response of the AFM, and the response of free spin clusters. The free spin magnetization is approximated by the Langevin function $L(x) = \coth(x) - 1/x$ which is the large S limit of the Brillouin function. The parameters n_c , S_{eff} and χ_{AF} are temperature dependent. From the cluster contribution, we expect a Curie law

$$\chi_0 = g^2 \mu_B^2 n_c(T) S_{\text{eff}}^2 / T \quad (2)$$

with $g = 2$, and where $n_c(T)$ is the density of clusters and S_{eff} is the size of the classical spin per cluster. In fig. 4 we plot the parameters n_c (closed circles), and S_{eff} (open circles) obtained from fits to the M vs B isotherms. We see that S_{eff} rises rapidly below 14 K with the number of clusters decreasing in a concomitant manner, such that their product (middle panel) remains a smooth function of T . Interestingly χ_{AF} shows a peak as expected for an AFM transition.

The free spin clusters giving a net magnetization have a typical size which depends on temperature. We estimate this cluster size N_c as scaling with its total moment S_{eff} by $N_c \sim S_{\text{eff}}/\alpha_m$, where the temperature-independent parameter α_m is the fraction of the moment per site that contributes to the FM net magnetization. The estimated cluster size $N_c = S_{\text{eff}}/\alpha_m$ should be distinguished from the density of clusters, n_c , which in principle is an independent quantity. Interestingly, the product $n_c N_c \alpha_m = n_c S_{\text{eff}}$ shows a strikingly simple temperature

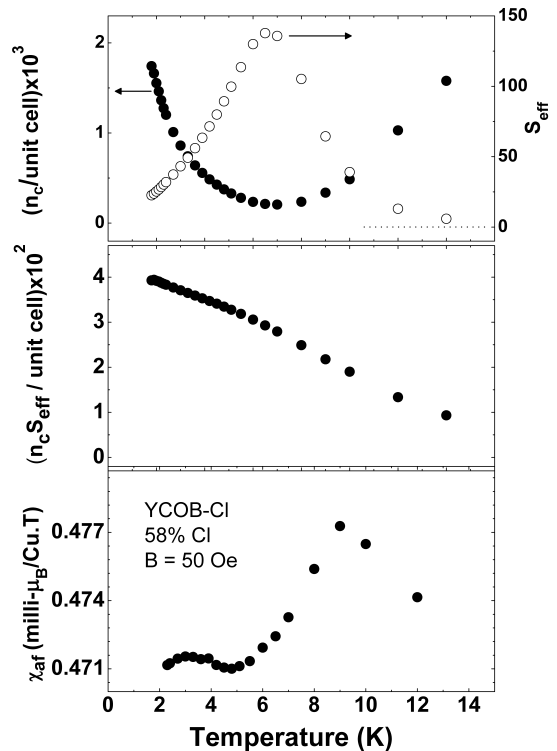


FIG. 4. Parameters obtained through fits to isotherms as in Fig. 2 using Eqn. 2. Top panel shows n_c (closed circles) and S_{eff} (open circles). Middle panel shows the product of n_c and S_{eff} which varies smoothly throughout the measured temperature range. Bottom panel shows χ_{AF} .

dependence (Figure 4 bottom panel). Above 7 K, we interpret $f_c = n_c N_c$ as the fraction of all magnetic sites that participate in the clusters. (Below 7 K, The domain size is history dependent, and depends on whether the system is field cooled or zero field cooled; N_c may then be interpreted as the square of the correlation length.) Long range ferrimagnetic order at 7 K is triggered when $f_c \approx 1$. At 7 K we find that $n_c S_{\text{eff}} \approx 0.03$, implying $\alpha_m \approx 0.03$, i.e. each spin cluster moment arises from the combination of a few dozen lattice sites.

III. MINIMAL MODEL FOR ANTICHRAL AFM ORDER WITH IN-PLANE CANTING

Above we showed that a distribution of spin clusters can explain the observed experimental data. In the following sections we will present a semi-microscopic theory that explains how such clusters can arise. We find that clusters are generated by combining two ingredients. (1) ABH disorder, which expands the regime of short-ranged antichiral ordering. (2) Certain anisotropic beyond-Heisenberg spin exchanges, especially a kagome Kitaev-type exchange [24] expected to be present here, which produce FM canting and hence generate clusters

of FM moments from short range order. Before going to the details of that discussion, in this section we first give a brief review of the possible magnetic ordering in the clean kagome limit with more conventional Heisenberg and DM interaction and discuss the relevant ordering pattern for the current material.

The most dominant symmetry allowed spin exchange Hamiltonian on ideal single layer kagome lattice can be written as [25],

$$H = J \sum_{\langle ij \rangle} S_i \cdot S_j + D_z \sum_{\langle ij \rangle} (S_i \times S_j)_z + \dots \quad (3)$$

where the first and the second term denote the isotropic Heisenberg and anisotropic DM interaction with DM vector being perpendicular to the kagome plane, and “...” denote other symmetry allowed couplings which will be discussed later. Note that the DM coupling is allowed due to the lack of inversion symmetry about the kagome bond centre, and its strength is linearly proportional to the spin-orbit coupling (λ), $|D_z| \propto \lambda J$ [25]. For the Heisenberg only term, the model is frustrated and favors a coplanar 120° AFM states on the kagome network at low temperatures via order by disorder. On the other hand, the DM term selects states with specific handedness among that subspace via a finite temperature phase transition. For $D_z > 0$, the “chiral” structures are chosen which preserve the C_3 rotation symmetry of the kagome lattice about the midpoint of a triangle, see Fig. 5 (b). The symmetry acts on both the spin and spatial (spin-orbit coupled) indices of the magnetic degrees of freedom. For $D_z < 0$, “antichiral” structures are chosen which do not have any physical C_3 rotation symmetry, see Fig. 5 (c). (If spin and space were decoupled, it would have rotations act oppositely on spin and on space; but this is unphysical.)

The consideration of the crystal field environment around the magnetic sites generically breaks the mirror symmetry about the pure kagome plane, and allows the in-plane DM terms (perpendicular to the kagome bonds, see Fig. 5(a)) in the above Hamiltonian. Although they also appear at the linear order in spin-orbit coupling, they are much weaker than the out-of-plane DM term (because they arise from inter-plane effects), hence their effects on the chiral and antichiral states can be computed perturbatively. For the chiral states, the in-plane terms generate a out-of-plane canting of the spins leading to a net FM moment perpendicular to the kagome plane. The relevant material showing no out-of-plane magnetization then rules out the possibility of the chiral order. The antichiral states, on the other hand, shows no out-of-plane canting with the in-plane DM terms. This can be clearly seen from a symmetry argument: the in-plane DM vectors transform oppositely under C_3 rotations compared to the antichiral spin order. Thus there is no energy gain due to the DM term for canting and the cost due to the Heisenberg exchange forbids it.

Focusing now on the antichiral state, we look for a mechanism for in-plane canting as observed in experi-

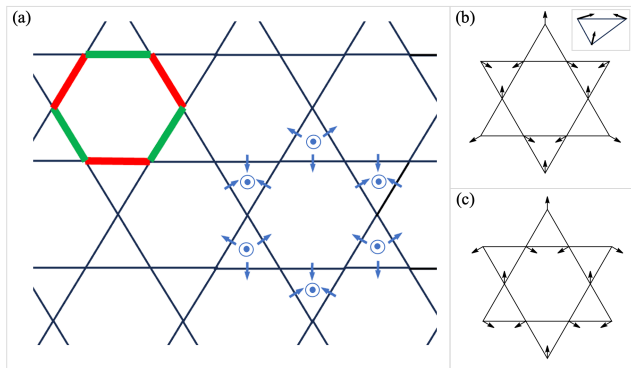


FIG. 5. Magnetic ordering in kagome lattice due to Heisenberg and DM interaction. (a) kagome network with dilute Alternating-Bond-Hexagon (ABH) defects shown with thick red/green bonds hosting stronger/weaker exchange couplings respectively. (ABH also appear with red/green interchanged, i.e. $2\pi/6$ rotated.) The blue arrows show in-plane DM vectors on each bond. The blue dots denote the out-of-plane DM vector on the surrounding bonds. To define the sign of DM vectors, bonds are oriented counterclockwise around each hexagon, or equivalently, clockwise around each triangle. (b) Chiral magnetic order for $D_z > 0$. Inset shows the ferromagnetic canting due to in-plane DM coupling. (c) Antichiral magnetic order for $D_z < 0$. This is the magnetic order considered below and relevant to the material, which has no out-of-plane canting.

ment. In-plane DM terms cannot generate such canting because the DM energy remains insensitive to any in-plane FM moment. (This is true even for the chiral state.) Therefore, we must look for other symmetry allowed couplings that must be added to Eq. 3. We will come back to this discussion in Section V. But before that we first turn to discussion of disorder effects on the antichiral state.

IV. GENERATING SPIN CLUSTERS, PART 1: SHORT RANGE ORDER VIA ALTERNATING-BOND-HEXAGON (ABH) DISORDER

The dilute density of ABH disorder on the kagome network is depicted in Fig. 5(a) with the red and green showing bonds with stronger and weaker spin exchange couplings. As described earlier, such alternation of coupling strength arises due to the random substitution of Br site by OH both above and below the kagome hexagons.

To understand the role of ABH disorder we consider a fully quantum 12 site model consisting of a star of David surrounding an ABH, and diagonalize it exactly. Focussing a single ABH is justified if we assume a dilute density of ABH in the system. Every ABH is then locally surrounded by the pristine kagome which we further assume hosts an at least short-range antichiral order. We incorporate this surrounding short-ranged order in the model by applying a mean-field b on the outer vertices of

the star of David containing the ABH consistent with the surrounding antichiral pattern (see bottom right inset of Fig. 6). This leads to the following 12-site Hamiltonian:

$$H = H_{\text{Heis}} + \sum_{i=7}^{12} \mathbf{b}_i \cdot \mathbf{S}_i + \Delta J H_{\Delta J}$$

$$H_{\Delta J} = \left(\sum_{\langle ij \rangle \in \text{strong}} \mathbf{S}_i \cdot \mathbf{S}_j - \sum_{\langle ij \rangle \in \text{weak}} \mathbf{S}_i \cdot \mathbf{S}_j \right) \quad (4)$$

where H_{Heis} is the isotropic Hamiltonian on all the bonds as described in Eq. 3, $H_{\Delta J}$ is the heisenberg exchange on strong minus weak bonds on the central hexagon, and \mathbf{b}_i are the mean-fields assigned on the outer vertices of the star of David as shown on the bottom right inset of Fig. 6. We assume their magnitude remains same for all the vertices, $|\mathbf{b}_i| = b$. We then investigate the consequence of such mean field on the spins on the ABH. In Fig. 6, we show the average magnitude of the spin expectation vector on the hexagon, $|S|_{\text{avg}} = \frac{1}{6} \sum_{i=1}^6 |\langle \mathbf{S}_i \rangle|$ as a function of mean-field. There are two distinct effects observed, associated with complementary mechanisms, which we tentatively refer to as “classical” and “quantum”.

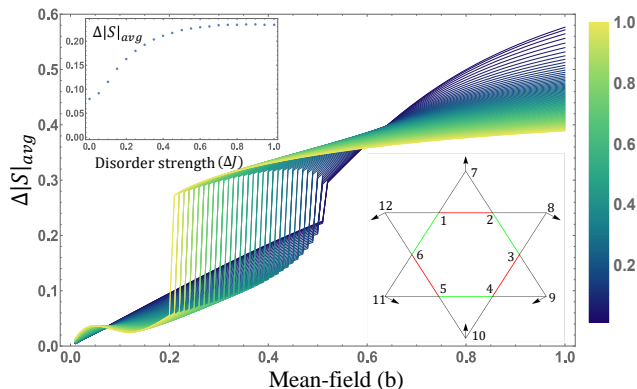


FIG. 6. Exact diagonalization of 12-spin Hamiltonian on a star of David with ABH: Inset on the bottom right shows the star of David with ABH and mean-field assigned on outer vertices consistent with antichiral pattern. Red and green lines show strong and weak bonds with strength $J + \Delta J$ and $J - \Delta J$ (assuming ΔJ positive), respectively. The black arrows on the outer vertices represent the effective mean-field acting on those sites due to the short-ranged antichiral AFM order on its surrounding. In the main figure, average norm of the ground state expectation values of the spins on the ABH, $|S|_{\text{avg}} = \frac{1}{6} \sum_{i=1}^6 |\langle \mathbf{S}_i \rangle|$, is shown as a function of antichiral order mean-field. Each curve of the plot are obtained by setting a fixed value of disorder strength. The maximum of the physical mean-field considered is $2J(|S|_{\text{avg}}) < 1$. The sharp jump in $|S|_{\text{avg}}$ represents the location of the level crossing. The inset of the top left shows the variation of the change of $|S|_{\text{avg}}$ at the level crossing with disorder strength.

Classical mechanism: relieved classical frustration. There are two sources of the frustration on kagome lattice: frustration inherent to the kagome geometry leading

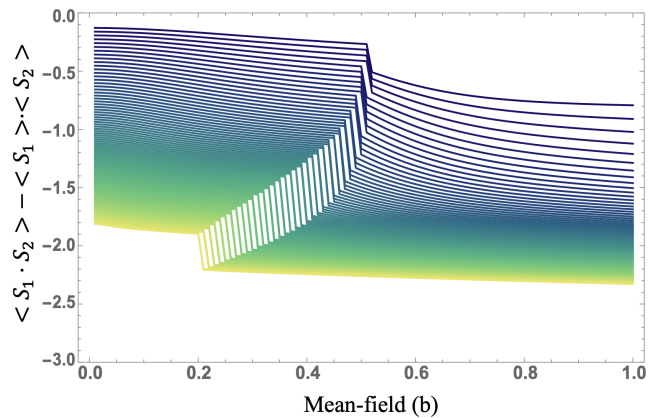


FIG. 7. Quantum fluctuations of the bond energies on strong bonds: For a perfect singlet and triplet, values of the above quantities are -3 and 1, respectively. With increasing the disorder strength, the strong bond becomes more of singlet character.

to various possibilities of competing orders, and frustration due to the competing interactions. The kagome lattice with equal nearest-neighbor couplings is frustrated already for classical Heisenberg interactions. In this scenario, the small DM coupling in addition to the Heisenberg interaction favors the antichiral states partially relieving the frustration. The ABH, on the other hand, incorporating the stronger and weaker couplings, modifies the classical energy (per bond) of the classical antichiral order from $J/2$ to $J/2 - \Delta J^2/6J$. Such energy modification is associated with the local FM canting of the spins on the disordered triangles, indicating further reduction of frustration. However, this local canting arising from ABH gives no net coarse-grained FM moment, but rather a larger-scale AFM pattern (see SI for details). The local reduction of frustration around the ABH can potentially help to set in short-range ordering on the ABH more easily than the rest of the pristine kagome, leading to the cluster model which has been introduced phenomenologically in the earlier sections. This effect is also seen when including quantum effects in exactly diagonalizing the 12-site ABH model: at larger $b/J > 0.2$, (sufficiently away from the classical ordered limit, $b/J < 0.5$) the classical spin moment $|S|_{\text{avg}}$ is greatly enhanced by ΔJ , with a positive jump arising with a level crossing with increasing ΔJ (Fig. 6). Phenomenologically, this enhanced $|S|_{\text{avg}}$ can be interpreted as a local enhancement of short-range order near each ABH. An interesting corollary of the above effect can be the pinning of density of the short-ranged cluster to that of the ABH, which might be worth understanding experimentally.

Quantum mechanism: enhanced singlet formation. Now considering quantum effects in full, it is clear that ABH supports singlet formation on the strong bonds, in addition to any other effects. Such singlet formation can successfully compete against classical orders: even the most naive valence bond solid states which

consist of singlets on strong bonds and free spins elsewhere on ABH enjoy an energy per bond of $J/2 - \Delta J/2$. This effect is seen in the 12-site ABH model: at small $b/J \lesssim 0.2$ the classical spin moment $|S|_{\text{avg}}$ is suppressed by ΔJ (Fig. 6), and at any b the strong bonds support increasing quantum fluctuations in the bond energy ($\langle S_i \cdot S_j \rangle - \langle S_i \rangle \cdot \langle S_j \rangle$) with ΔJ (Fig. 7). Phenomenologically, this enhanced quantum fluctuation can result in suppression of long-range classical order and enhanced regime of short-range order arising from ABH. Such effects are especially quite significant near the $T_N \sim 14$ K, where the short-range order is weak enough. At much lower temperatures, the mean field due to the short-ranged domains enhances, leading to long-range ordered phase at $T^* \sim 7$ K. Clearly, the quantum effect of ABH can be thought of as stretching the domain of short-ranged ordering in the material.

V. GENERATING SPIN CLUSTERS, PART 2: IN-PLANE FM CANTING VIA KITAEV EXCHANGES

Having discussed the origin of the short-range cluster, we now turn back to the origin of the weak FM moments on such clusters. As we already established the necessity to look for interactions beyond the Heisenberg and DM terms in Sec. III, we must now look for additional anisotropic symmetric exchanges that are allowed on the kagome lattice.

In presence of spin-orbit coupling, such exchanges can be obtained in a standard manner [26]. Given the DM vector on a bond connecting site i and j being \hat{D}_{ij} , the easy axis anisotropic interaction is $\propto 1/J (S_i \cdot \hat{D}_{ij}) (S_j \cdot \hat{D}_{ji})$. Clearly, such term varies quadratically with the spin-orbit coupling and remains weak compared to other exchanges described in Section III. Since the net DM vector in kagome is a linear combination of out-of-plane (perpendicular to kagome plane) and in-plane (perpendicular to the kagome bond) component (see Fig. 5(a)), it leads to various terms in the anisotropic exchange interaction, among which the dominant contribution to the canting moment comes from the Kitaev-type bond dependent interaction [24].

$$H_{\text{Kitaev}} = J_{\text{Kitaev}} \sum_{\langle ij \rangle \mu} S_i^\mu S_j^\mu \quad (\mu = X, Y, Z) \quad (5)$$

where the details of the easy axes X , Y and Z of the Kitaev interaction are given in the SI. We note that the Kitaev interaction explicitly breaks the continuous $U(1)$ symmetry. Expanding the classical Kitaev energy around the antichiral state perturbatively within a single triangle ($q = 0$) analysis appropriate for this $q = 0$ order, we

obtain:

$$\frac{H_{\text{Kitaev}}}{J_{\text{Kitaev}}} \approx -\frac{1}{2} + \frac{1}{6} (a \cos(2\phi_1) + b \sin(2\phi_1)) + \mathcal{O}(a^2, b^2, ab), \quad (6)$$

where a and b denote the in-plane deviations of the spin configuration from antichiral order:

$$\phi_2 - \phi_3 = \frac{2\pi}{3} + \frac{a}{\sqrt{3}}, \quad \phi_2 + \phi_3 - 2\phi_1 = 2\pi + b, \quad (7)$$

and, ϕ_1, ϕ_2, ϕ_3 are the angel variables measured from the x -axis, describing any in-plane spin configuration with the indices defined in the anticlockwise manner (As an illustrative example, see the triangle formed by sites 7, 1 and 2 in bottom right inset of Fig. 6). Note that the leading term in the energy is a ϕ_1 independent constant, which implies although the Kitaev term breaks the $U(1)$ explicitly, there is still an emergent $U(1)$ invariance in the antichiral subspace. The classical Kitaev energy is minimized by the following spin configurations:

$$\begin{aligned} J_{\text{Kitaev}} > 0 \text{ (AFM)} &: f_1 = 2\phi_1 + \pi, & (8) \\ J_{\text{Kitaev}} < 0 \text{ (FM)} &: f_1 = 2\phi_1, & (9) \end{aligned}$$

where, $f_1 = \tan^{-1}(b/a)$. Clearly, the canting configuration is tied to the overall symmetry breaking angle ϕ_1 . The net canted moment on the triangle is given by

$$m = \begin{cases} \frac{1}{2} \{ \cos \phi_1, -\sin \phi_1 \}, & \text{for FM Kitaev} \\ \frac{1}{2} \{ -\cos \phi_1, \sin \phi_1 \}, & \text{for AFM Kitaev} \end{cases} \quad (10)$$

Note that the above canting remains uniform as long as there is a uniform antichiral ordering set by the symmetry breaking angle ϕ_1 . In the absence of true long-range ordering, even if there is a short-ranged antichiral state present over a cluster, the Kitaev interaction thus generate a net FM moment on it, which is a crucial component to the observed thermodynamic behavior.

We note that another possibility of the in-plane canting could in principle potentially arise from the ABH disorder itself. However, as described earlier (also see in details in the SI), due to the C_3 rotation symmetry of the ABH, the resultant FM moment of the triangles forms a vortex configuration with zero average moment per hexagon.

VI. DISCUSSION

The identification of the salient experimental features of a quantum spin liquid state is an ongoing effort. In the above we have presented comprehensive results on a new system, $\text{YCu}_3(\text{OH})_6[(\text{Cl}_x\text{Br}_{(1-x)})_{3-y}(\text{OH})_y]$, in which replacing Br by sufficient Cl (i.e. tuning x) a magnetic state can be tuned in. This substitution as well as the presence of the $(\text{OH})^-$ ions necessarily introduces disorder. In the regime of disordered ABH density where there is an AFM ordered state we find evidence for the

formation of FM clusters. We develop a theory for the origin of these clusters in the present setting, via disorder and Kitaev interactions.

Going beyond the magnetically ordered case towards a possible nearby Dirac QSL phase, we anticipate a complementary mechanism for generating FM moments from certain 120^0 AFMs. For a Dirac QSL, chiral time reversal symmetry breaking with FM spin clusters generates a mass term for fermion bilinears, leading monopoles to proliferate and destroy the QSL; on the kagome lattice, the expected magnetic order is then 120^0 AFM [27]. This suggests that a proximate Dirac QSL could support a linear coupling between 120^0 AFM and FM moments through the monopole effects.

We note also a possible relation to ferromagnetic clusters seen on the Dirac spin liquid candidate samples. These are the compounds in the YCOB-Cl family that show no magnetic order and may be spin liquid candidates, namely those with $x < 0.4$ and associated higher density of ABH disorder. Recent work [17] found that the unusual magnetization could be explained through ferromagnetic spin clusters arising in the candidate spin liquid regime. These possibly-delocalized clusters can be viewed as counterparts of emergent random singlets but

with a dominant effect from ferromagnetic interactions that can arise via the interplay of frustrated antiferromagnetic interactions in a strong-disorder RG. It would be interesting to consider how increasing ABH disorder may interplay with a phase transition into a Dirac QSL, and what the role of ferrimagnetic or ferromagnetic spin clusters may be across such a transition.

VII. ACKNOWLEDGEMENTS

IK acknowledges support by the U.S. Department of Energy Office of Science, Award Number DE-SC0025478. The work at the University of Virginia (BSS and TDF) was supported by U.S. National Science Foundation Award DMR-2016909. PL acknowledges support by U.S. Department of Energy office of Basic Sciences Grant No. DE-FG02-03ER46076. SL acknowledges support by the National Key Research and Development Program of China (Grants No. 2022YFA1403400 and No. 2021YFA1400401), and Chinese Academy of Sciences (Grants No. XDB33000000 and No. GJTD-2020-01). The work at the Naval Research Laboratory (J.P.) has been funded by the Office of Naval Research, under the NRL 6.1 Base Program.

-
- [1] M.R. Norman, Colloquium: Herbertsmithite and the search for the quantum spin liquid, *Rev. Mod. Phys.* **88**, 041002, 2016.
- [2] Wei Sun, Ya-Xi Huang, Sergiy Nokhrin, Yuanming Panb and Jin-Xiao Mi, Perfect Kagomé lattices in $YCu_3(OH)_6Cl_3$: a new candidate for the quantum spin liquid state, *J. Mater. Chem. C*, **4**, 8772-8777 (2016).
- [3] A. Zorko, M. Pregelj, M. Klanjšek, M. Gomilšek, Z. Jagličić, J. S. Lord, J. A. T. Verezhak, T. Shang, W. Sun, and J.-X. Mi, Coexistence of magnetic order and persistent spin dynamics in a quantum kagome antiferromagnet with no intersite mixing, *Phys. Rev. B*, **99**, 214441, (2019).
- [4] A. Zorko, M. Pregelj, M. Gomilšek, M. Klanjšek, O. Zaharko, W. Sun, and J.-X. Mi, Negative-vector-chirality 120^0 spin structure in the defect- and distortion-free quantum kagome antiferromagnet $YCu_3(OH)_6Cl_3$, *Phys. Rev. B*, **100**, 144420, (2019).
- [5] T. Arh, M. Gomilšek, P. Prelovšek, M. Pregelj, M. Klanjšek, A. Ozarowski, S. J. Clark, T. Lancaster, W. Sun, J.-X. Mi, and A. Zorko, Origin of Magnetic Ordering in a Structurally Perfect Quantum Kagome Antiferromagnet, *Phys. Rev. Lett.* **125**, 027203 (2020).
- [6] B. Bernu, L. Pierre, K. Essafi, and L. Messio, Effect of perturbations on the kagome $S = \frac{1}{2}$ antiferromagnet at all temperatures, *Phys. Rev. B*, **101**, 140403 (2020).
- [7] L. Messio, O. Cépas, and C. Lhuillier, Schwinger-boson approach to the kagome antiferromagnet with Dzyaloshinskii-Moriya interactions: Phase diagram and dynamical structure factors, *Phys. Rev. B*, **81**, 064428 (2010).
- [8] O. Cépas, C.M.Fong, P.W.Leung, and C.Lhuillier, Quantum phase transition induced by Dzyaloshinskii-Moriya interactions in the kagome antiferromagnet, *Phys. Rev. B*, **78**, 140405(R) (2008).
- [9] M. Hering and J. Reuther, Functional renormalization group analysis of Dzyaloshinsky-Moriya and Heisenberg spin interactions on the kagome lattice, *Phys. Rev. B*, **95**, 054418 (2017).
- [10] Quentin Barthelemy, Pascal Pupha, Katharina M. Zoch, Cornelius Krellner, Hubertus Luetkens, Christopher Baines, Denis Sheptyakov, Edwin Kermarrec, Philippe Mendels, and Fabrice Bert, Local study of the insulating quantum kagome antiferromagnets, *Phys. Rev. Matls*, **3**, 074401, 2019.
- [11] Xiaochen Hong, Mahdi Behnami, Long Yuan, Boqiang Li, Wolfram Brenig, Bernd Büchner, Yuesheng Li, and Christian Hess, Heat transport of the kagome Heisenberg quantum spin liquid candidate $YCu_3(OH)_{6.5}Br_{2.5}$, Localized magnetic excitations and a putative spin gap, *Phys. Rev. B*, **106**, L220406, (2022).
- [12] Fangjun Lu, Long Yuan, Jian Zhang, Boqiang Li, Yongkang Luo and Yuesheng Li, The observation of quantum fluctuations in a kagome Heisenberg antiferromagnet, *Nature Comm. Phys.*, **5**, 272, 1, 2022.
- [13] X. H. Chen, Y. X. Huang, Y. Pan, and J. X. Mia, Quantum spin liquid candidate With an almost perfect kagome layer, $YCu_3(OH)_6Br_2[Br_x(OH)_{(1-x)}]$, *J. Magn. Mater.* **512**, 167066 (2020).
- [14] Zhenyuan Zeng, Xiaoyan Ma, Si Wu, Hai-Feng Li, Zhen Tao, Xingye Lu, Xiao-hui Chen, Jin-Xiao Mi, Shi-Jie Song, Guang-Han Cao, Guangwei Che, Kuo Li, Gang Li, Huiqian Luo, Zi Yang Meng, and Shiliang Li, Pos-

- sible Dirac quantum spin liquid in the kagome quantum antiferromagnet, *Phys. Rev. B*, (Letter), **105**, L121109 (2022).
- [15] S. Suetsugu, T. Asaba, S. Ikemori, Y. Sekino, Y. Kasahara, K. Totsuka, B. Li, Y. Zhao, Y. Li, Y. Kohama, Y. Matsuda, Gapless spin excitations in a quantum spin liquid state of $S=1/2$ perfect kagome antiferromagnet, arXiv preprint 2407.16208 (2024).
- [16] Aini Xu, Qinxin Shen, Bo Liu, Zhenyuan Zeng, Lankun Han, Liqin Yan, Jun , Luo, Jie Yang, Rui Zhou, and Shiliang Li, Magnetic ground states in the kagome system $YCu_3(OH)_6 [(Cl_xBr_{1-x})_{3-y}(OH)_y]$, *Phys. Rev. B* **110**, 085146 (2024).
- [17] B. S. Shivaram, Joseph C. Prestigiacomo, Aini Xu, Zhenyuan Zeng, Trevor D. Ford, Itamar Kimchi, Shiliang Li, and Patrick A. Lee, Nonanalytic magnetic response and intrinsic ferromagnetic clusters in a kagome spin-liquid candidate, *Phys. Rev. B* **110**, L121105 (2024).
- [18] J. Liu, L. Yuan, X. Li, B. Li, K. Zhao, H. Liao, and Y. Li, Gapless spin liquid behavior in a kagome Heisenberg antiferromagnet with randomly distributed hexagons of alternate bonds, *Phys. Rev. B*, **105**, 024418 (2022).
- [19] Zhenyuan Zeng, Chengkang Zhou, Honglin Zhou, Lankun Han, Runze Chi, Kuo Li, Maiko Kofu, Kenji Nakajima, Yuan Wei, Wenliang Zhang, Daniel G. Mazzone, Zi Yang Meng and Shiliang Li, Spectral evidence for Dirac spinons in a kagome lattice antiferromagnet, *Nature Physics* volume 20, pages 1097–1102 (2024).
- [20] Ying Ran, Michael Hermele, Patrick A. Lee, and Xiaogang Wen, Projected-Wave-Function Study of the Spin-1/2 Heisenberg Model on the Kagomé Lattice, *Phys. Rev. Lett*, **98**, 117205 (2007).
- [21] Michael Hermele, Ying Ran, Patrick A. Lee, and Xiaogang Wen, Properties of an algebraic spin liquid on the kagome lattice, *Phys. Rev. B*, **77**, 224413 (2008).
- [22] P. Puphal, M. Bolte, D. Sheptyakov, A. Pustogow, K. Kliemt, M. Dressel, M. Baenitz, and C. Krellner, Strong magnetic frustration in $Y_3Cu_9(OH)_{19}Cl_8$: A distorted kagome antiferromagnet, *J. Mater. Chem. C*, **5**, 2629 (2017).
- [23] Dipranjan Chatterjee, Pascal Puphal, Quentin Barthélemy, Jannis Willwater, Stefan Süllo, Christopher Baines, Sylvain Petit, Eric Ressouche, Jacques Ollivier, Katharina M. Zoch, Cornelius Krellner, Michael Parzer, Alexander Riss, Fabian Garmroudi, Andrej Pustogow, Philippe Mendels, Edwin Kermarrec, and Fabrice Bert, From spin liquid to magnetic ordering in the anisotropic kagome Y-kapellasite $Y_3Cu_9(OH)_{19}Cl_8$: A single-crystal study, *Phys. Rev. B*, **107**, 125156 (2023).
- [24] Itamar Kimchi, and Ashvin Vishwanath, Kitaev-Heisenberg models for iridates on the triangular, hyperkagome, kagome, fcc, and pyrochlore lattices, *Phys. Rev. B* **89**, 014414 (2014).
- [25] M. Elhadj, B. Canals, and C. Lacroix, Symmetry breaking due to Dzyaloshinsky-Moriya interactions in the kagome lattice, *Phys. Rev. B*, **66**, 014422, 2002.
- [26] T. Moriya, Anisotropic Superexchange Interaction and Weak Ferromagnetism, *Phys. Rev.* **120**, 91, 1960.
- [27] Xue-Yang Song, Chong Wang, Ashvin Vishwanath, and Yin-Chen He, Unifying description of competing orders in two-dimensional quantum magnets. *Nat Commun* **10**, 4254 (2019).

SUPPLEMENTARY MATERIAL: Disorder-induced spin-cluster ferrimagnetism in a doped kagome spin liquid candidate

Arnab Seth¹, Joseph C. Prestigiacomo², Aini Xu³, Zhenyuan Zeng^{3,4}, Trevor D. Ford⁵,
B.S. Shivaram⁵, Shiliang Li^{3,4,6}, Patrick A. Lee⁷, and Itamar Kimchi¹

¹*School of Physics, Georgia Institute of Technology, Atlanta, Georgia 30332, USA.*

²*Materials Science and Technology Division, Naval Research Laboratory, Washington, DC 20375, USA.*

³*Beijing National Laboratory for Condensed Matter Physics, Institute of Physics, Chinese Academy of Sciences, Beijing 100190, China.*

⁴*School of Physical Sciences, University of Chinese Academy of Sciences, Beijing 100190, China.*

⁵*Department of Physics, University of Virginia, Charlottesville, Virginia 22904, USA.*

⁶*Songshan Lake Materials Laboratory, Dongguan, Guangdong 523808, China*

⁷*Department of Physics, Massachusetts Institute of Technology, Cambridge, Massachusetts 02139, USA.*

(November 18, 2024)

A Canting due to bond-Ising or Kitaev terms

In this section, we consider two potential perturbation to the Heisenberg Hamiltonian which are bond-Ising interaction and Kitaev interaction. Both of these interactions have similar symmetry, and they break continuous $U(1)$ symmetry of the Heisenberg Hamiltonian. Via a single triangle ($\mathbf{q} = 0$) classical analysis, we show that such terms indeed favor a uniform FM canting of the underlying antichiral AFM order.

Since we are considering $q=0$ magnetic orders, it is enough to look at a single triangle. The bond-Ising and Kitaev terms are given by:

$$H_{\text{Ising}} = J_{\text{Ising}} \sum_{\langle ij \rangle} (S_i \cdot (\mathbf{r}_i - \mathbf{r}_j)) (S_j \cdot (\mathbf{r}_i - \mathbf{r}_j)) \quad (1)$$

$$H_{\text{Kitaev}} = J_{\text{Kitaev}} \sum_{\langle ij \rangle_\mu} S_i^\mu S_j^\mu \quad (\mu = X, Y, Z) \quad (2)$$

$$X = \left\{ -\frac{1}{\sqrt{6}}, \frac{1}{\sqrt{2}}, \frac{1}{\sqrt{3}} \right\}, \quad Y = \left\{ -\frac{1}{\sqrt{6}}, -\frac{1}{\sqrt{2}}, \frac{1}{\sqrt{3}} \right\}, \quad Z = \left\{ \sqrt{\frac{2}{3}}, 0, \frac{1}{\sqrt{3}} \right\} \quad (3)$$

where in the last line X, Y and Z of the Kitaev interaction are given in terms of the reference axes (x, y, z) described in Fig. 1. We note that although both the terms break the continuous $U(1)$ symmetry, there is still an emergent $U(1)$ symmetry in the antichiral subspace. Here we perturbatively compute the classical energy of the above two Hamiltonian around the anti-chiral state. For this we define,

$$\theta_2 - \theta_3 = \frac{2\pi}{3} + \frac{a}{\sqrt{3}} \quad , \quad \theta_2 + \theta_3 - 2\theta_1 = 2\pi + b \quad (4)$$

Note that the scaling of a and b is chosen such that when Eq. 4 is substituted in the classical Heisenberg energy, the leading order correction becomes $\propto (a^2 + b^2)$. Solving θ_2 and θ_3 from the above two equations, we can substitute them in the classical energy expression for the bond-Ising and Kitaev terms. Expanding in powers of a and b , we obtain (here we express the classical energies in the units of the corresponding exchange interaction scale):

$$\begin{aligned} \frac{H_{\text{Ising}}}{J_{\text{Ising}}} &= \frac{1}{4} \left[-2 \cos(2\theta_1 + b) + \sqrt{3} \cos \left(2\theta_1 + \frac{b}{2} + \frac{a}{2\sqrt{3}} - \frac{\pi}{6} \right) \right. \\ &+ \cos \left(2\theta_1 + \frac{b}{2} - \frac{a}{2\sqrt{3}} - \frac{2\pi}{3} \right) + 2 \sin \left(\frac{a}{2\sqrt{3}} - \frac{b}{2} - \frac{\pi}{6} \right) + 2 \sin \left(\frac{a}{2\sqrt{3}} + \frac{b}{2} - \frac{\pi}{6} \right) \\ &\left. - 2 \sin \left(\frac{a}{\sqrt{3}} + \frac{\pi}{6} \right) + \sin \left(2\theta_1 + \frac{a}{2\sqrt{3}} + \frac{b}{2} - \frac{\pi}{6} \right) + \sqrt{3} \sin \left(2\theta_1 - \frac{a}{2\sqrt{3}} + \frac{b}{2} + \frac{2\pi}{3} \right) \right] \quad (5) \end{aligned}$$

$$\approx -\frac{3}{4} + \frac{1}{4} (a \cos(2\theta_1) + b \sin(2\theta_1)) + \mathcal{O}(a^2, b^2, ab) \quad (6)$$

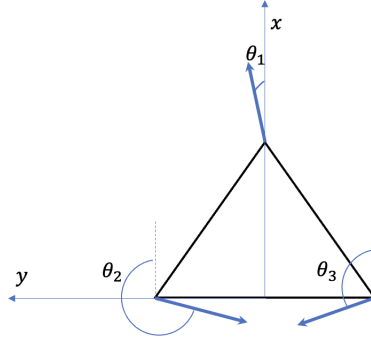


Figure 1: Reference axes for a single triangle classical analysis. Note that in the main text all the angles (ϕ_i) are measured from vertical axis. Therefore, the two conventions are related by: $\phi_i = \theta_i + \pi/2$

$$\begin{aligned} \frac{H_{\text{Kitaev}}}{J_{\text{Kitaev}}} &= \frac{1}{6} \left(2 \cos(b + 2\theta_1) - \sqrt{3} \cos\left(\frac{1}{6}(\sqrt{3}a + 3b - \pi + 12\theta_1)\right) \right) \\ &\quad - \cos\left(\frac{1}{6}(-\sqrt{3}a + 3b + 4\pi + 12\theta_1)\right) + 2 \sin\left(\frac{1}{6}(\sqrt{3}a - 3b - \pi)\right) + 2 \sin\left(\frac{1}{6}(\sqrt{3}a + 3b - \pi)\right) \\ &\quad - 2 \sin\left(\frac{1}{\sqrt{3}}a + \frac{\pi}{6}\right) - \sin\left(\frac{1}{6}(\sqrt{3}a + 3b - \pi + 12\theta_1)\right) - \sqrt{3} \sin\left(\frac{1}{6}(-\sqrt{3}a + 3b + 4\pi + 12\theta_1)\right) \end{aligned} \quad (7)$$

$$\approx -\frac{1}{2} - \frac{1}{6} (a \cos(2\theta_1) + b \sin(2\theta_1)) + \mathcal{O}(a^2, b^2, ab) \quad (8)$$

Note that θ_1 independent constant term is the consequence of the emergent $U(1)$ invariance in the antichiral subspace. Substituting:

$$a = r \cos(f_1) \quad , \quad b = r \sin(f_1) \quad (9)$$

We get:

$$H_{\text{Ising}}/J_{\text{Ising}} \approx -\frac{3}{4} + \frac{1}{4}r \cos(f_1 - 2\theta_1) + \mathcal{O}(a^2, b^2, ab) \quad (10)$$

$$H_{\text{Kitaev}}/J_{\text{Kitaev}} \approx -\frac{1}{2} - \frac{1}{6}r \cos(f_1 - 2\theta_1) + \mathcal{O}(a^2, b^2, ab) \quad (11)$$

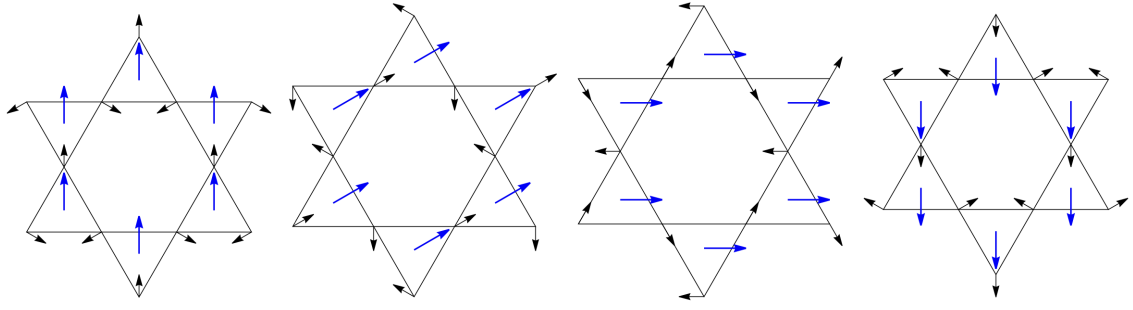
Note that the classical energy is minimized by,

$$J_{\text{Ising}} < 0 \text{ (FM)} : f_1 = 2\theta_1 \quad , \quad J_{\text{Ising}} > 0 \text{ (AFM)} : f_1 = 2\theta_1 + \pi \quad (12)$$

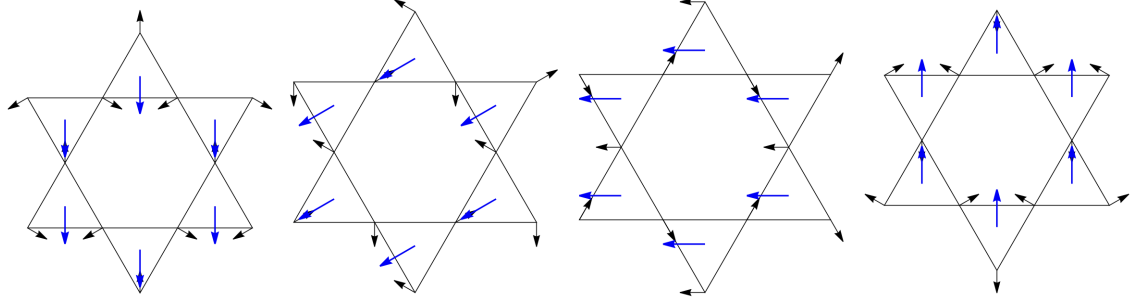
$$J_{\text{Kitaev}} > 0 \text{ (AFM)} : f_1 = 2\theta_1 \quad , \quad J_{\text{Kitaev}} < 0 \text{ (FM)} : f_1 = 2\theta_1 + \pi \quad (13)$$

The Ising and Kitaev term give rise to opposite kind of canting. Note that the $U(1)$ symmetry breaking decides the canting angle of the spin, hence the net canting moment on the triangle. The net canted moment on the triangle is given by,

$$m = \begin{cases} \frac{1}{2} \{\cos(\theta_1) , -\sin(\theta_1)\} , & \text{for FM Ising and AFM Kitaev} \\ \frac{1}{2} \{-\cos(\theta_1) , \sin(\theta_1)\} , & \text{for AFM Ising and FM Kitaev} \end{cases} \quad (14)$$



(a) Various spin orientations and associated canting for AFM Kitaev or FM bond-Ising interaction



(b) Various spin orientations and associated canting for FM Kitaev or AFM bond-Ising interaction

Figure 2: Canting due to the bond-Ising and Kitaev interaction: The black arrows on the kagome vertices represent the spins of the corresponding antichiral order. The blue arrows on the centres of each triangles represent the net moment of the corresponding triangles. (a) and (b) show the canting due to AFM (FM) and FM (AFM) Kitaev (bond-Ising) interaction. Four figures on each panel show different configurations of the canting moment due to different antichiral patterns, given by $\theta_1 = 0, \pi/3, \pi/2, \pi$.

We can parameterize the canted moment as,

$$m = \frac{1}{2} \{ \cos(\gamma), \sin(\gamma) \} \quad (15)$$

Then we find that for AFM (FM) bond-Ising (Kitaev), $\gamma = -\theta_1$ and AFM (FM) bond-Ising (Kitaev) gives time-reversed canted moments, $\gamma = -\theta_1 + \pi$. Note that θ_1 is the global choice of the antichiral order which breaks the $U(1)$ symmetry of the Heisenberg model and DM interaction. In Fig. 2, we plot the net FM moments due to the bond-Ising and Kitaev term (both FM and AFM) on a star of David of the kagome lattice for different choices of θ_1 . Note that although both terms generate similar canting, the magnitude of their effect depends on the coupling constant of these two terms. Generically, for the kagome lattice with DM anisotropy, it is expected that Kitaev interaction is more dominant than the other anisotropic exchanges. Therefore, in the main text, we only discuss the Kitaev interaction leaving aside the contribution from bond-Ising term.

B Canting due to strong bond disorder

In this section, we describe the local canting due to ABH disorder from the $\mathbf{q} = 0$ single triangle classical analysis. Note that, depending on the density of the ABH, there can be two different disordered triangles possible: triangles with one of the bond either stronger or weaker than the other two (occurs even for

a single isolated ABH), and triangles with all the three bonds are of different strength (occurs only for adjacent ABH). The spin Hamiltonians for these two cases are given by:

$$H_{ABH,1} = H_{\text{Heisenberg}} + H_{\text{DMz}} + \Delta J S_2 \cdot S_3 \quad (16)$$

$$H_{ABH,2} = H_{\text{Heisenberg}} + H_{\text{DMz}} + \Delta J (S_2 \cdot S_3 - S_1 \cdot S_2) \quad (17)$$

For reference of the labels of the spins, see Fig. 1. We note that both of the above Hamiltonian do not break global $U(1)$ invariance. Hence we measure the angle of S_2 and S_3 from S_1 . The antichiral AFM order (atleast short ranged) is established by the combination of $H_{\text{Heisenberg}}$ and H_{DMz} , before the onset of the FM canting. Therefore, we treat the disorder term perturbatively around the antichiral states. We assume:

$$\theta_2 = \frac{4\pi}{3} + \delta_{ABH}, \quad \theta_3 = \frac{2\pi}{3} - \delta_{ABH}, \quad (18)$$

where δ_{ABH} denotes the amount of FM canting due to ABH disorder(see Fig. 1). Substituting the above in the classical energy expression, and solving their minima, we obtain:

- For $H_{ABH,1}$ (isolated ABH):

$$\delta_{ABH,1} = \begin{cases} -\frac{\pi}{3} & \text{for } \Delta J < -0.5 \\ i \left(\log(4) - \log \left(\frac{(i+\sqrt{3})(-i-i\Delta J + \sqrt{(1+\Delta J)^2(3+4\Delta J(2+\Delta J))})}{2(1+\Delta J)^2} \right) \right) & \text{for } \Delta J > -0.5 \end{cases} \quad (19)$$

The net moment of the triangle can be computed as:

$$m_{ABH,1} = 1 + 2 \cos \left(\frac{4\pi}{3} + \delta_{ABH,1} \right) = \begin{cases} -1 & \text{for } \Delta J < -0.5 \\ \frac{\Delta J}{1+\Delta J} & \text{for } \Delta J > -0.5 \end{cases} \quad (20)$$

- For $H_{ABH,2}$ (adjacent ABH):

$$\delta_{ABH,2} = \begin{cases} -\frac{\pi}{3} & \text{for } \Delta J < -0.4 \\ \tan^{-1} \left(\frac{\sqrt{3}(-2+\Delta J(\Delta J-1) + \sqrt{(1+\Delta J)^2(2+\Delta J)(2+5\Delta J)})}{(2+\Delta J - \Delta J^2 + 3\sqrt{(\Delta J+1)^2(\Delta J+2)(5\Delta J+2)})} \right) & \text{for } \Delta J > -0.4 \end{cases} \quad (21)$$

The net moment of the triangle is given by:

$$m_{ABH,2} = 1 + 2 \cos \left(\frac{4\pi}{3} + \delta_{ABH,2} \right) = \begin{cases} -1 & \text{for } \Delta J < -0.4 \\ \frac{3\Delta J}{2+2\Delta J} & \text{for } \Delta J > -0.4 \end{cases} \quad (22)$$

Note that the qualitative results obtained in the above two cases are very similar. The difference lies in the detailed values of the canted moment. In Fig. 3, we plot the net FM moment of the triangle for the both the kinds of disorder. In Fig. 4, we show the FM canting of the triangles surrounding the ABH (star of David). Note that due to a C_3 symmetry of the ABH hexagon, the canted configuration also has a C_3 rotation symmetry, leading to zero net moment on each such hexagons. Interestingly, the

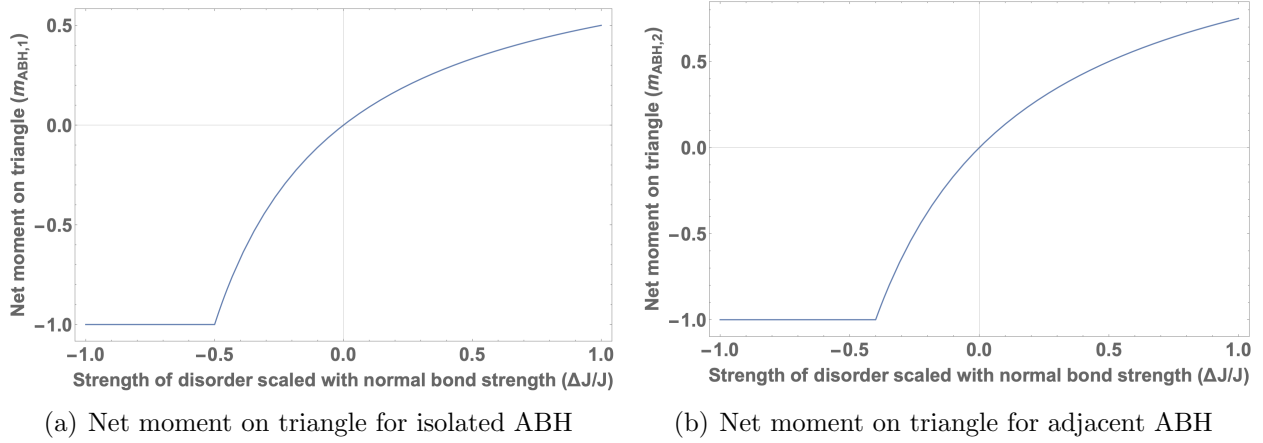
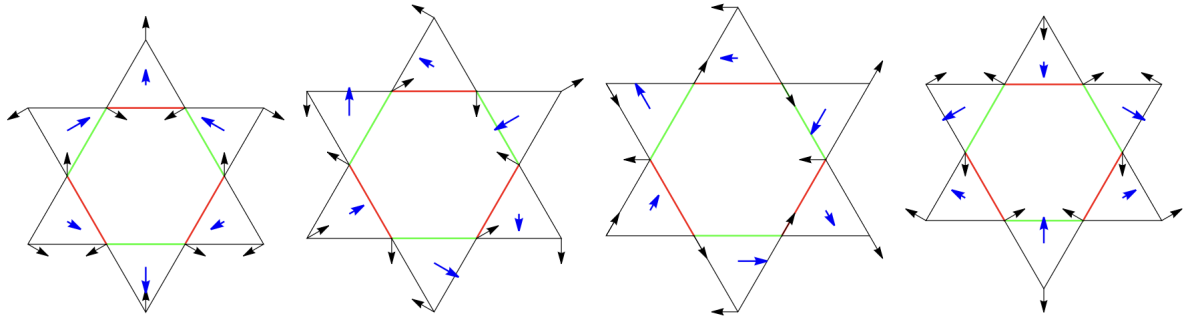
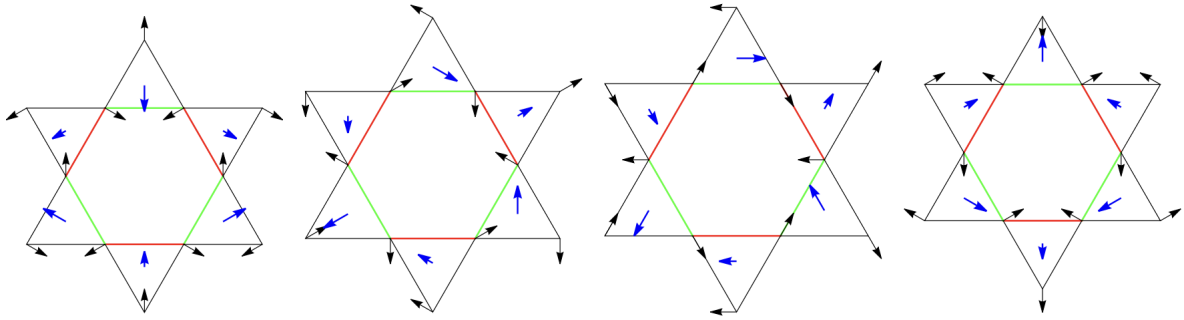


Figure 3: Net magnetic moment of a single triangle with ABH disorder: (a) shows net moment on triangles having two bonds of same strength, and one bond different from the others ($H_{ABH,1}$). (b) shows moment of triangles having all three bond strength different from each other ($H_{ABH,2}$). (b) occurs if two ABH are adjacent. We find that (b) is not qualitatively different from (a), so in the case where most ABH are dilute, getting some adjacent ABH does not give any qualitatively new effects, and we can safely ignore it below.

canted moments due to ABH forms a vortex configuration with vorticity -1, which is a consequence of the underlying antichiral pattern.



(a) Various spin orientations and associated canting for strong bond on top ABH



(b) Various spin orientations and associated canting for weak bond on top ABH

Figure 4: Canting due to the ABH disorder: Red and green bonds are stronger ($J + \Delta J$) and weaker ($J - \Delta J$) bonds, respectively with the choice of $\Delta J/J = 0.25$ for all figures. The black arrows on the kagome vertices represent the spins of the corresponding antichiral order. The blue arrows on the centres of each triangles represent the net moment of the corresponding triangles. (a) and (b) show two different possibilities of ABH with red or green bond being on the top of the hexagon, respectively. The two configurations are related by a C_3 symmetry. Four figures on each row show different configurations due to $\theta_1 = 0, \pi/3, \pi/2, \pi$. Note that the blue arrows (net moments) always forms a vortex configuration with vorticity -1.